# $CoSe_2$@N-Doped Graphene Nanocomposite High-Efficiency Counter Electrode For Dye-Sensitized Solar Cells

**Tansir Ahamad** ( tahamed@ksu.edu.sa )
King Saud University https://orcid.org/0000-0002-9400-5317

**Research Article**

**Keywords:** Dye-sensitized solar cell, Counter electrode, CoSe2, N-Doped Graphene

**Posted Date:** December 28th, 2021

**DOI:** https://doi.org/10.21203/rs.3.rs-1197256/v1

# Abstract

Photovoltaics is defined as a group of solar cells that convert solar energy into electricity. Among these cells, dye-sensitized solar cells (DSSCs) have received considerable attention due to of their low cost and high efficiency for energy conversion. In present study, $CoSe_2$@N-doped graphene nanocomposite has been prepared in an inert atmosphere and used as a DSSC counter electrode. The fabricated nanocomposite was characterised using analytical techniques including FTIR, TGA, XRD, Raman, XPS, and BET. The assembled DSSC obtains a photoelectric conversion efficiency (PCE) of 7.65%, which is higher than the PCE (7.19%) of the Pt electrode assembly cell under the same conditions. The promising performance of the fabricated counter electrodes may be due to the excellent surface area of the nanocomposites, the doping of hetroatomes which provide the active sites to boost the catalytic activities towards $I_3^-$ reduction.


# Introduction

The sun has long been the most important renewable energy source on earth and the researchers are trying to utilize this vital source of energy for the benefit of humans. Even though, the world's biggest oil exporter, Saudi Arabia, has also pledged to cut its carbon emissions to net zero by 2060 and the plans and objective of Vision 2030, Saudi Arabia has focused on producing 50 percent of its electricity from renewable sources by 2030 to meet the growing demand for energy, and to provide favourable climatic conditions and suitable economic feasibility. Solar radiation can be converted directly into electricity by solar cells (photovoltaic cells) (Ahamad et al., 2021; Aldalbahi et al., 2021; Wang et al., 2021). Among these solar cells, dye-sensitized solar cells (DSSC) have attracted widespread attention due to their low cost, easy preparation, and high solar energy conversion efficiency (Hagfeldt et al., 2010; O'Regan and Grätzel, 1991). Generally, a typical DSSCs composed of a dye-adsorbed $TiO_2$ anode, a redox shuttle ($I_3^-/I^-$), and a counter electrode (CE). The function of CE is to collect the electron from the external circuit and catalyse the reduction of $I_3^-$ into $I^-$ (Jin et al., 2017; Leu et al., 2017; Meng et al., 2018). Pt is widely used as a counter electrode (CE) to fabricate DSSC due to its high conductivity and excellent catalytic activity towards $I_3^-$reduction, however, the limited resources and high price of Pt limits its industrial application (Hou et al., 2018; Yu et al., 2016). Therefore, current studies are focused on finding alternatives to Pt. Some non-Pt materials such as porous carbon have been used as counter electrode to fabricate the DSSC due to their large surface area, high conductivity, and low cost (Tapa et al., 2021; Yue et al., 2018). Moreover, several transition metal based compounds specially, transition metal selenides, such as $CoSe_2$, $NbSe_2$, $NiSe_2$, and $ZnSe_2$ have excellent catalytic activity towards $I_3^-$ reduction (Gao et al., 2018; Singh et al., 2017; Wang et al., 2016). Among these, cobalt selenide ($CoSe_2$) has attracted much attention because of its high catalytic activity, low cost and excellent long-term stability (Huang et al., 2018; Wang, X. et al., 2019; Yang et al., 2020). However, the electron conductivity of $CoSe_2$ is not meet to the required standard due to its semiconducting behaviour and poor conductivity (Chiu et al., 2016; Li et al., 2021; Ou et al., 2020). On the other hand, the carbon based materials such as graphite carbon, carbon

nanotubes, graphene and graphene oxide not only show the excellent electrical conductivity but also the high surface area to enhance the catalytic activity. Recently, it was noticed that the doping of the heteroatoms such as N and S into carbon provide the additional active sites, which enhance the charge transfer behaviour as well as enhance the catalytic activity of the nanocomposites (Ding et al., 2022; Su et al., 2022; Wei et al., 2022). Therefore, the nanocomposite based counter electrode materials have attracted wide attention because they combine the advantages of each component and help improve the catalytic activity and the stability of the electrode (Silambarasan et al., 2021; Wang et al., 2022; Zhao et al., 2021). Being inspired by the above investigations, here we have design low-cost, effective and environmentally friendly counter electrode for DSSC using $CoSe_2$@N-doped graphene nanocomposite. The electrode materials were characterized using FTIR, XRD, Raman, BET, XPS, SEM and TEM. The electrochemical performance of $CoSe_2$@N-doped graphene was analysed by electrochemical impedance spectroscopy (EIS), cyclic voltammetry (CV), and Tafel polarization curve, and the effects of N-doped graphene (NGN) loading with $CoSe_2$ were discussed in details. The DSSC fabricated using the $CoSe_2$/NGN-15 electrode exhibits excellent PCE value of 7.65% higher than that of other fabricated electrode even higher than that of the Pt electrode (7.19%) under the same experiment condition. This may be due to the synergetic effect between the $CoSe_2$ nanoparticles and graphene moreover the doping of the nitrogen into the graphene matrix also improve the DSSC performance and have good corrosion resistance to a corrosive redox electrolyte as CE materials. We hope that, the present work offers to fabricate Pt free counter electrode for DSSC and provides an opportunity to develop a highly efficient and low cost DSSC as the plans and objectives of Vision 2030.

## Experimental

# 2.1 Materials

Cobalt nitrate hexahydrate ($Co(NO_3)_2{\cdot}6H_2O$, Graphene, selenium powder, N719 dye, are from Sigma-Aldrich. Ethylene glycol, Ethanol, Potassium iodide (KI), and Iodine ($I_2$) were obtained from Merck, Germany. $TiO_2$ paste (TPP3, 20 nm; TPP200, 200 nm) and FTO glass (sheet resistance 15 Ω) were purchased from Dalian Seven Color Technology Co., Ltd.

# 2.2 Preparation of $CoSe_2$@NGN

The counter electrode materials were prepared as following; 20 mg of the NGN was dispersed into 50 mL ethanol and sonicated for 30 min., Then 0.40 mmol of $Co(NO_3)_2.6H_2O$ and then 26 mmol $(CH_3COO)Na$ were added to this mixture and stirred continuously. After that 0.80 mmol of $SeO_2$ was added to this solution and stirred again for 3 h, under $N_2$ gas, and then 4.92 mmol $NaBH_4$ dissolved in 20 mL ethanol was dropped to the above mixture and stirred overnight. The obtained precipitate was filtered, washed dried and then annealed at 400 $^oC$ for 4 h in $N_2$ atmosphere to remove amorphous selenium. Resulting product $CoSe_2$@NGN-20, was washed and saved for further uses. Other compositions were prepared

using similar procedure after changing the amount of NGN as 5, 10 and 15 as $CoSe_2$@NGN-5, $CoSe_2$@NGN-10 and $CoSe_2$@NGN-15 respectively.

# 2.3 Cell fabrication and measurement

The detailed of counter electrode (CE) and DSSC fabrication processes, material characterization, and electrochemical measurement could be found in the Supporting Information.

# Results And Discussion

The $CoSe_2$@NGN nanocomposite was prepared using reduction and post calcination method as shown in figure-1.

The FTIR spectra of the nanocomposites illustrate in figure 2(a) and the peaks at 1567 $cm^{-1}$ and 1647 $cm^{-1}$ assigned to the C=C and C=N bonds. Other peaks at 1334, 1402, and 1054 $cm^{-1}$ peak are assigned to the C-O, C–N, and C–O–C stretching, respectively (Ahamad et al., 2020a; Ahamad et al., 2019). While the peaks in the region of 3170-3382 $cm^{-1}$ are corresponding to N–H, -$NH_2$, and O–H bonds, respectively and the FTIR peak at 587 $cm^{-1}$ support the bond Co-Se. The thermal stability of the nanocomposites was determine using TGA analysis and the results were illustrated in the figure 2(b). The TGA outcomes revealed that as the amount of the NGN was increased from 5–20% the thermal stability of the nanocomposites was decreased and the reduced weight was found to be 49.02%, 41.64%, 38.43% and 34.88% corresponding to $CoSe_2$@NGN-5, $CoSe_2$@NGN-10, $CoSe_2$@NGN-15 and $CoSe_2$@NGN-20 respectively at 800 $^oC$ (Ahamad and Alshehri, 2013; Naushad et al., 2015). The purity and the crystalline nature of the nanocomposites were also determine using XRD, as shown in figure 2(c), The diffraction peaks at 2θ = 30.78, 34.52, 35.96, 40.38, 47.72, 50.23, 53.48, 56.95 and 63.29 can be assigned to the (101), (111), (120), (210), (211), (002), (031), (131) and (122) planes are assigned to the orthorhombic $CoSe_2$ (PDF-53–0449). The doping of the nitrogen atoms into to the graphene and growing the $CoSe_2$ nanoparticles into the NGN matrix was further determine using Raman spectra. As shown in figure 2(d), two main Raman peaks were observed at 1354 $cm^{-1}$ and 1592 $cm^{-1}$ known as D and G bands, respectively. The G band assigned to the $sp^2$ hybridized C=C bonds, whereas the D band assigned to the $sp^3$ hybridized C-C bond (Ahamad et al., 2020c; Ahamad et al., 2020d; Alhokbany et al., 2020). The intensity of these two peaks increased with increasing the contents of NGN in to the nanocomposites. Other peaks at 163.46, 469.23 and 670.21 $cm^{-1}$ assigned to the $CoSe_2$ nanoparticles. The defect density of carbon is proportional to the value of $I_D/I_G$ and found to be 1.24 in the case of $CoSe_2$@NGN-15.

The results indicated that the doping of N atoms and the existence of $sp^3$ C-C and C-N bonds enhanced the disordered of graphene lattice. Which lead the electron transfer and catalytic efficiency for $I_3^-$ reduction in DSSC. The microstructure and the morphology of the fabricated electrode materials were determine using SEM and TEM techniques. As shown in figure 3(a), the SEM image of the $CoSe_2$@NGN-15 nanocomposite show the porous structure and grown the nanoparticles in the NGN matrix. The

enlarged pattern of the SEM image is shown in figure 3(b) and the results revealed that revealed that the spherical shaped $CoSe_2$ nanoparticles with the dimeter range of 20-50 nm are well dispersed into the NGN matrix. These results support that the fabricated electrode material contains hetrostructure which being conducive to the exposure the active sites at the surface of the catalyst to reduce the $I_3^-$. To deep understand the microstructural of $CoSe_2$@NGN-15, TEM analysis was used. As shown in figure 3(c), $CoSe_2$ nanoparticles with an average size of ~38.9 nm are uniformly embedded in the NGN matrix.

The HRTEM image as shown in figure 3(d), displayed inter-planar spacing of 0.29 nm, and 0.19 nm in the high-resolution TEM (HRETM) images are indexed to the (101), and (211) oriented facets of $CoSe_2$ nanoparticles. The inserted figure od selected area electron diffraction show the polycrystalline nature of the $CoSe_2$ nanoparticles. To porosity of the nanocomposites were further characterized using the nitrogen adsorption-desorption isotherm and the curves were illustrated in figure 4(a).

It was noticed that all the nanocomposites show type-IV hysteresis loops and demonstrating the mesoporous structure (Alshehri et al., 2017; Alshehri et al., 2016; Vinu et al., 2018). In the case of the $CoSe_2$@NGN-15, the hysteresis loops were observed from 0.40 to 0.99 and the specific surface area was found to be 421.0 $m^2/g$, while for $CoSe_2$@NGN-5, $CoSe_2$@NGN-10, $CoSe_2$@NGN-20 the surface area was found to be 440.2, 436.4 and 414.12 $m^2/g$ respectively. These results demonstrate that the surface area of the nanocomposites were increased with increasing the contents of NGN into the electrode materials. Figure 4(b) show the pore size dimeter was observed about in the range of 20-67 nm in the case of all the nanocomposites. The large surface area and nanoscale pore size of the $CoSe_2$@NGN based electrode materials not only support the additional catalytic sites but also enhance the electron transfer during the $I_3^-$ reduction. The elemental composition and the valance state of the elements present in the nanocomposite as monitored by XPS analysis, as shown in figure 5(a), the XPS spectra of $CoSe_2$@NGN-15 show the presence of C, N, Co, Se and O into the nanocomposite. As shown in figure 5(b), the C 1s peak was deconvoluted into four peaks and cantered at at 284.68, 285.71, 286.90 and 287.78 eV and assigned to the C-C, C-N, C=N, and O=C-O function groups presence into the NGN matrix.

The N1s spectra of the nanocomposites was split into three peaks and show the binding energy at into 398.24, 400.36, and 401.43 eV, corresponding to pyridinic, pyrrolic/pyridonic, and graphitic nitrogen functional groups respectively as shown in figure 5(c) (Ahamad et al., 2020b; Khalaf et al., 2020). The XPS peak of Co 2p was deconvoluted into four characteristic peaks as shown in figure 5(d), two of them are the main peaks and the binding energy cantered at 778.71 and 793.89 eV corresponding to the Co $2p_{3/2}$ and Co $2p_{1/2}$, respectively, and other two peaks were observed at binding energy 780.23 and 796.91 eV are assigned to the satellite peaks of Co $2p_{3/2}$ and Co2 $p_{1/2}$ respectively. Figure 5(e), shows the XPS spectrum of Se 3d and the main peak was split into two peaks and cantered at 54.74 and 55.83 eV and assigned to Se $3d_{3/2}$ and Se $3d_{5/2}$ respectively (Liu et al., 2016). The XPS results shows that the O atoms also present into the matrix and the O 1 s spectrum was deconvoluted into binding energies of 530.44, and 531.88 eV and assigned to the presence of C-O and Se-O bonds respectively.

# Photovoltaic Performance

The DSSC was fabricated as sandwich structure using the the N719 dye-loaded $TiO_2$ as a photo-anode, an iodine solution ($I_3^-/I^-$) as an electrolyte, and $CoSe_2$@NGN (or Pt) as a counter electrode. The current density voltage curve (J–V) of the fabricated DSSCs using $CoSe_2$@NGN-5, $CoSe_2$@NGN-10, $CoSe_2$@NGN-15, and $CoSe_2$@NGN-20 and Pt under 100 mW/cm$^2$ AM 1.5 G are illustrated in figure 6(a). The values of photovoltaic factors including short circuit current density ($J_{sc}$), open circuit voltage ($V_{oc}$), filling factor (FF) and maximum power ($P_{max}$) are summarized in table-1. It was observed that DSSC fabricated using $CoSe_2$@NGN-15, show excellent photovoltaic performance than other electrode materials prepared in this study. The short-circuit photocurrent ($J_{sc}$) of DSSC fabricated using $CoSe_2$@NGN-15 CE was found to be 15.40 mA/cm$^2$, higher than that of $CoSe_2$@NGN-5 (13.58 mA/cm$^2$), $CoSe_2$@NGN-10 (14.21 mA/cm$^2$), and $CoSe_2$@NGN-20 (15.10 mA/cm$^2$), even outperforming that of Pt CEs (14.56 mA/cm$^2$). The higher value of the $J_{sc}$ is help to boost the reduction of $I_3^-$ and dye regeneration (Niu et al., 2018; Wang, Q. et al., 2019). The open-circuit voltage ($V_{oc}$), fill factor (FF) and the PCE was found to be 0.74 V, 66.45% and 7.65% respectively for $CoSe_2$@NGN-15, while these values were obtained about to 0.74, 66.10%, 7.19% with Pt counter electrode. The excellent performance of $CoSe_2$@NGN-15 can be attributed due to the synergetic effect between $CoSe_2$ nanoparticles and NGN matrix, because the NGN matrix has excellent conductivity and the uniformly dispersed $CoSe_2$ nanoparticles provide excellent catalytic activity for $I_3^-$ reduction.

**Table 1**: PCE values and relevant parameters of the different CEs

| Counter Electrode | $J_{sc}$ (mA cm$^{-2}$) | $V_{oc}$ (V) | FF (%) | PCE (%) |
|---|---|---|---|---|
| $CoSe_2$@NGN-5 | 13.58 | 0.731 | 66.73 | 6.62 |
| $CoSe_2$@NGN-10 | 14.21 | 0.755 | 67.77 | 7.27 |
| $CoSe_2$@NGN-15 | 15.40 | 0.745 | 66.66 | 7.65 |
| $CoSe_2$@NGN-20 | 15.10 | 0.757 | 64.32 | 7.35 |
| Pt | 14.56 | 0.746 | 66.10 | 7.19 |

Moreover, the $CoSe_2$@NGN-15 nanocomposite has proper distribution as well as as greater the specific surface area of the counter electrode, and the higher the catalytic activity, and the better the photovoltaic performance of DSSC. On the other hand, the nanocomposites $CoSe_2$@NGN-5 and $CoSe_2$@NGN-10 show the DSSC performance lower than that of Pt. Based on the above results the proposed photovoltaic mechanism of the $CoSe_2$@NGN-5 CE is illustrated in Figure 7.

# Electrochemical Performance Of Ce Materials

The relationship between the photoelectric conversion efficiency of the fabricated DSSC with the counter electrode was further carried out using CV, EIS and Tafel plots. As shown in figure 8(a), the cyclic voltammetry cure of the DSSC fabricated using $CoSe_2$@NGN-5, $CoSe_2$@NGN-10, $CoSe_2$@NGN-15, and $CoSe_2$@NGN-20 and Pt show the peaks due to the redox reaction of $I_3^-$ as: $I_3^- + 2e^- \rightarrow 3I^-$ (i) and $3I_2 + 2e^- \rightarrow 2I_3^-$ (ii). It was noticed that the the current density (J) and the potential ($\Delta E_{pp}$) difference between the two peaks are important factors for comparing the catalytic activity of different CE materials. It was observed that the CE based on $CoSe_2$@NGN-15 nanocomposite show higher current density and lower peaks difference than these of Pt, indicating that $CoSe_2$@NGN-15 has superior catalytic ability than Pt for $I_3^-$reduction (Kavan et al., 2011; Swami et al., 2015). The stability experiment was carried out using CV cycles as shown in figure 8(b), and the outcomes revealed that after 50 cycles on 50 mV/sec scan rate, the current density, peak positions and $E_{PP}$ value is substantially unchanged, indicating $CoSe_2$@NGN-15 having excellent electrochemical stability.

The electrocatalytic activity of the $CoSe_2$@NGN-5, $CoSe_2$@NGN-10, $CoSe_2$@NGN-15, and $CoSe_2$@NGN-20 and Pt electrode were further determine using the Tafel polarization curves asillustrated in figure 8(c). All the Tafel polarization plots were divided into three zones, first the polarization zone occurs due to the electrochemical reaction and noticed at low over potential (|V| <120 mV), in the second zone is sharp slope is and it is Tafel zone, in which, the current density($J_o$) is changed and noticed at moderate over-potentials (120 mV < |V| < 400 mV), third is the limiting diffusion zone, which depend on the transport of ions and occurs at high over-potential (|V|> 400 mV), and used to determine the limiting diffusion current density ($J_{lim}$). The value of of $J_o$ and $J_{lim}$ related to the catalytic activity of the counter electrode. As shown in figure 8(c), it has been noticed that $CoSe_2$@NGN-15 has a higher value of $J_o$ as compared to Pt based CE, resulting shown higher catalytic activity towards $I_3^-$ reduction, and the higher $J_{lim}$ value of $CoSe_2$@NGN-15, indicate that $CoSe_2$@NGN-15 based CE has a faster ion diffusion rate than standard Pt CE (Roy-Mayhew et al., 2010). The electrochemical impedance spectroscopy (EIS) measurements of the DSSC fabricated using $CoSe_2$@NGN-5, $CoSe_2$@NGN-10, $CoSe_2$@NGN-15, and $CoSe_2$@NGN-20 and Pt based CE is illustrated in figure 8(d). The EIS results used to determine various resistances, charge-transfer between the interface of electrode/electrolyte and the catalytic efficiency of the counter electrode.

The EIS Nyquist plots, show three semicircles, the $R_s$ is represent to resistance between the FTO and CE materials, the $R_{ct-1}$ is representing to the charge transfer resistance between the electrolyte and CEs and the $R_{ct-2}$ represents the electron transfer resistance between the $TiO_2$/electrolyte and the dye. It was noticed that in all the Nyquist plots the value of $R_{ct-2}$ is unchanged and almost similar, these results may have been due to the use of similar type photoanaode materials. While the value of $R_s$ and $R_{ct-1}$ was changed. The results reveal that $CoSe_2$@NGN-15 show almost similar value of Rs to the Pt and support that these is a good connection between the FTO glass and the electrode materials. While the $R_{ct-1}$ value of $CoSe_2$@NGN-15 was found to be lower, than that of other electrodes even lower than that of Pt based CE. On the other hand, it was noticed that the the $CoSe_2$@NGN-15 nanocomposite show lower value of

Nernst diffusion impedance ($Z_w$) than the Pt base CE for diffusion of $I^-/I_3^-$ redox couple within the electrolyte (Kavan et al., 2011; Swami et al., 2015). This may be due to the existence of active site to contact with the electrolyte without any hindrances and resulting show excellent photoelectric conversion efficiency in the fabricated DSSC.

## Conclusion

Sustainability has been the focus of researcher vision; therefore, we have fabricated novel counter electrode materials for DSSC using $CoSe_2$ nanoparticles embedded into NGN. The fabricated nanocomposites $CoSe_2$@NGN were characterized using several analytical techniques. The experimental results show that the $CoSe_2$@NGN electrode has excellent catalytic activity. Among them, the DSSC assembled by $CoSe_2$@NGN-15 obtains 7.65% PCE, which is higher than that of the DSSC assembled with Pt electrode (7.19%). The influence of different film thickness on the photovoltaic performance of DSSC was studied and discussed in depth. The excellent performance of $CoSe_2$@NGN-15 is attributed due to the synergetic effect of $CoSe_2$ nanoparticles and N-doped graphene matrix, because the N-doped graphene exhibit excellent conductivity and uniformly dispersed $CoSe_2$ which boost the catalytic activity of the nanocomposites. The preparation of this new type of non-Pt material provides a new method for DSSCs counter electrode research and promotes its industrialization process to utilised the sustainable solar energy for the benefit of humans.

## Declarations

# 6. Acknowledgement

The authors thanks to Researchers Supporting Project number (RSP-2021/6), King Saud University, Riyadh, Saudi Arabia.

## References

1. T. Ahamad, A. Aldalbahi, S.M. Alshehri, S. Alotaibi, S. Alzahly, Z.-B. Wang, P.X. Feng, Enhanced photovoltaic performance of dye-sensitized solar cells based Ag2O doped BiFeO3 hetrostructures. Sol. Energy **220**, 758–765 (2021)
2. T. Ahamad, S.M. Alshehri, Thermal degradation and evolved gas analysis of epoxy (DGEBA)/novolac resin blends (ENB) during pyrolysis and combustion. J. Therm. Anal. Calorim. **111**(1), 445–451 (2013)
3. T. Ahamad, M. Naushad, S.I. Al-Saeedi, S.M. Alshehri, N/S-doped carbon embedded with AgNPs as a highly efficient catalyst for the reduction of toxic organic pollutants. Mater. Lett. **264**, 127310 (2020a)

4. T. Ahamad, M. Naushad, A.N. Alhabarah, S.M. Alshehri, N/S doped highly porous magnetic carbon aerogel derived from sugarcane bagasse cellulose for the removal of bisphenol–A. Int. J. Biol. Macromol. **132**, 1031–1038 (2019)
5. T. Ahamad, M. Naushad, S.M. Alshheri, Fabrication of highly porous N/S doped carbon embedded with CuO/CuS nanoparticles for NH3 gas sensing. Mater. Lett. **268**, 127515 (2020b)
6. T. Ahamad, M. Naushad, Y. Alzaharani, S.M. Alshehri, Photocatalytic degradation of bisphenol-A with g-C3N4/MoS2-PANI nanocomposite: kinetics, main active species, intermediates and pathways. J. Mol. Liq. **311**, 113339 (2020c)
7. T. Ahamad, M. Naushad, R.H. Mousa, N. Khalaf, S.M. Alshehri, Synthesis and characterization cobalt phosphate embedded with N doped carbon for water splitting ORR and OER. Journal of King Saud University-Science **32**(6), 2826–2830 (2020d)
8. A. Aldalbahi, T. Ahamad, S.M. Alshehri, Z.-B. Wang, P.X. Feng, *Three-dimensional architectures composed of two-dimensional atomic layer molybdenum disulphide for solar cell and self-powered photodetectors with improved performance* (Energy Exploration & Exploitation, 2021), p. 01445987211036828
9. N.S. Alhokbany, M. Naushad, V. Kumar, S.M. Alshehri, T. Ahamad, Self-nitrogen doped carbons aerogel derived from waste cigarette butts (cellulose acetate) for the adsorption of BPA: Kinetics and adsorption mechanisms. Journal of King Saud University-Science **32**(8), 3351–3358 (2020)
10. S.M. Alshehri, J. Ahmed, A.N. Alhabarah, T. Ahamad, T. Ahmad, Nitrogen-doped cobalt ferrite/carbon nanocomposites for supercapacitor applications. ChemElectroChem **4**(11), 2952–2958 (2017)
11. S.M. Alshehri, A. Aldalbahi, A.B. Al-Hajji, A.A. Chaudhary, in het Panhuis, M., Alhokbany, N., Ahamad, T., 2016. Development of carboxymethyl cellulose-based hydrogel and nanosilver composite as antimicrobial agents for UTI pathogens. Carbohydrate polymers 138, 229-236
12. I.T. Chiu, C.T. Li, C.P. Lee, P.Y. Chen, Y.H. Tseng, R. Vittal, K.C. Ho, Nanoclimbing-wall-like CoSe2/carbon composite film for the counter electrode of a highly efficient dye-sensitized solar cell: A study on the morphology control. Nano Energy **22**, 594–606 (2016)
13. K. Ding, J. Hu, J. Luo, W. Jin, L. Zhao, L. Zheng, W. Yan, B. Weng, H. Hou, X. Ji, 2022. Confined N-CoSe2 active sites boost bifunctional oxygen electrocatalysis for rechargeable Zn–air batteries. Nano Energy 91
14. C. Gao, Q. Han, M. Wu, Review on transition metal compounds based counter electrode for dye-sensitized solar cells. Journal of Energy Chemistry **27**(3), 703–712 (2018)
15. A. Hagfeldt, G. Boschloo, L. Sun, L. Kloo, H. Pettersson, Dye-sensitized solar cells. Chem. Rev. **110**(11), 6595–6663 (2010)
16. Q. Hou, J. Ren, H. Chen, P. Yang, Q. Shao, M. Zhao, X. Zhao, H. He, N. Wang, Q. Luo, Z. Guo, 2018. Synergistic Hematite-Fullerene Electron-Extracting Layers for Improved Efficiency and Stability in Perovskite Solar Cells. ChemElectroChem 5(5), 726-731
17. S. Huang, H. Wang, S. Wang, Z. Hu, L. Zhou, Z. Chen, Y. Jiang, X. Qian, Encapsulating CoS2-CoSe2 heterostructured nanocrystals in N-doped carbon nanocubes as highly efficient counter electrodes for

dye-sensitized solar cells. Dalton Trans. **47**(15), 5236–5244 (2018)

18. Z. Jin, M. Zhang, M. Wang, C. Feng, Z.S. Wang, Metal Selenides as Efficient Counter Electrodes for Dye-Sensitized Solar Cells. Acc. Chem. Res. **50**(4), 895–904 (2017)
19. L. Kavan, J.H. Yum, M. Grätzel, Optically transparent cathode for dye-sensitized solar cells based on graphene nanoplatelets. ACS Nano **5**(1), 165–172 (2011)
20. N. Khalaf, T. Ahamad, M. Naushad, N. Al-Hokbany, S.I. Al-Saeedi, S. Almotairi, S.M. Alshehri, Chitosan polymer complex derived nanocomposite (AgNPs/NSC) for electrochemical non-enzymatic glucose sensor. Int. J. Biol. Macromol. **146**, 763–772 (2020)
21. Y.A. Leu, M.H. Yeh, L.Y. Lin, T.J. Li, L.Y. Chang, S.Y. Shen, Y.S. Li, G.L. Chen, W.H. Chiang, J.J. Lin, K.C. Ho, Thermally Stable Boron-Doped Multiwalled Carbon Nanotubes as a Pt-free Counter Electrode for Dye-Sensitized Solar Cells. ACS Sustainable Chemistry and Engineering **5**(1), 537–546 (2017)
22. W. Li, M. Zheng, Z. Tian, G. Long, S. Zhang, Q. Chen, Q. Zhong, 2021. Coral-like CoSe2-nitrogen-doped porous carbon as efficient counter electrodes for quantum dot sensitized solar cells. ECS Journal of Solid State Science and Technology 10(4)
23. K. Liu, F. Wang, K. Xu, T.A. Shifa, Z. Cheng, X. Zhan, J. He, CoS2xSe2(1-x) nanowire array: An efficient ternary electrocatalyst for the hydrogen evolution reaction. Nanoscale **8**(8), 4699–4704 (2016)
24. X. Meng, C. Yu, X. Song, J. Iocozzia, J. Hong, M. Rager, H. Jin, S. Wang, L. Huang, J. Qiu, Z. Lin, Scrutinizing Defects and Defect Density of Selenium-Doped Graphene for High-Efficiency Triiodide Reduction in Dye-Sensitized Solar Cells. Angewandte Chemie - International Edition **57**(17), 4682–4686 (2018)
25. M. Naushad, T. Ahamad, Z.A. Alothman, M.A. Shar, N.S. AlHokbany, S.M. Alshehri, Synthesis, characterization and application of curcumin formaldehyde resin for the removal of Cd2+ from wastewater: kinetics, isotherms and thermodynamic studies. J. Ind. Eng. Chem. **29**, 78–86 (2015)
26. Y. Niu, X. Qian, J. Zhang, W. Wu, H. Liu, C. Xu, L. Hou, Stepwise synthesis of CoS2-C@CoS2 yolk-shell nanocages with much enhanced electrocatalytic performances both in solar cells and hydrogen evolution reactions. Journal of Materials Chemistry A **6**(25), 12056–12065 (2018)
27. B. O'Regan, M. Grätzel, A low-cost, high-efficiency solar cell based on dye-sensitized colloidal TiO2 films. Nature **353**(6346), 737–740 (1991)
28. J.H. Ou, B.N. Hu, S.Y. He, Y. Han, Metal-organic framework thin-film derived CoSe2/N co-doped carbon film as an efficient counter electrode for dye-sensitized solar cells. Chinese Journal of Inorganic Chemistry **36**(9), 1683–1689 (2020)
29. J.D. Roy-Mayhew, D.J. Bozym, C. Punckt, I.A. Aksay, Functionalized graphene as a catalytic counter electrode in dye-sensitized solar cells. ACS Nano **4**(10), 6203–6211 (2010)
30. K. Silambarasan, S. Harish, K. Hara, J. Archana, M. Navaneethan, Ultrathin layered MoS2 and N-doped graphene quantum dots (N-GQDs) anchored reduced graphene oxide (rGO) nanocomposite-based counter electrode for dye-sensitized solar cells. Carbon **181**, 107–117 (2021)
31. E. Singh, K.S. Kim, G.Y. Yeom, H.S. Nalwa, Two-dimensional transition metal dichalcogenide-based counter electrodes for dye-sensitized solar cells. RSC Advances **7**(45), 28234–28290 (2017)

32. H. Su, L. Lu, M. Yang, F. Cai, W. Liu, M. Li, X. Hu, M. Ren, X. Zhang, Z. Zhou, 2022. Decorating CoSe2 on N-doped carbon nanotubes as catalysts and efficient polysulfides traps for Li-S batteries. Chemical Engineering Journal 429
33. S.K. Swami, N. Chaturvedi, A. Kumar, R. Kapoor, V. Dutta, J. Frey, T. Moehl, M. Grätzel, S. Mathew, M.K. Nazeeruddin, Investigation of electrodeposited cobalt sulphide counter electrodes and their application in next-generation dye sensitized solar cells featuring organic dyes and cobalt-based redox electrolytes. J. Power Sources **275**, 80–89 (2015)
34. A.R. Tapa, W. Xiang, A.S.A. Ahmed, S. Wu, B. Li, Q. Liu, C.M.J. Chuti, X. Zhao, Porous rGO/ZnSe/CoSe2dispersed in PEDOT:PSS as an efficient counter electrode for dye-sensitized solar cells. Materials Chemistry Frontiers **5**(6), 2702–2714 (2021)
35. M. Vinu, D.S. Raja, Y.-C. Jiang, T.-Y. Liu, Y.-Y. Xie, Y.-F. Lin, C.-C. Yang, C.-H. Lin, S.M. Alshehri, T. Ahamad, Effects of structural crystallinity and defects in microporous Al-MOF filled chitosan mixed matrix membranes for pervaporation of water/ethanol mixtures. J. Taiwan Inst. Chem. Eng. **83**, 143–151 (2018)
36. Q. Wang, Y. Wang, P. Wei, X. Liu, L. Duan, One-step hydrothermal synthesis of In2.77S4 nanoparticles doped graphene oxide hybrids as efficient counter electrodes in dye-sensitized solar cells. Appl. Surf. Sci. **494**, 1–7 (2019)
37. W. Wang, X. Zuo, Q. Yang, Q. Yang, H. Tang, H. Zhang, G. Li, 2022. Constructing Fe/Fe3C nanocrystals with Fe-Nx sites in Fe–N–C electrocatalyst to achieve high performance for solar cells. Applied Catalysis B: Environmental 300
38. X. Wang, Y. Xie, B. Bateer, K. Pan, X. Zhang, J. Wu, H. Fu, CoSe 2 /N-Doped Carbon Hybrid Derived from ZIF-67 as High-Efficiency Counter Electrode for Dye-Sensitized Solar Cells. ACS Sustainable Chemistry and Engineering **7**(2), 2784–2791 (2019)
39. X. Wang, Y. Xie, B. Bateer, K. Pan, Y. Zhou, Y. Zhang, G. Wang, W. Zhou, H. Fu, Hexagonal FeS nanosheets with high-energy (001) facets: Counter electrode materials superior to platinum for dye-sensitized solar cells. Nano Research **9**(10), 2862–2874 (2016)
40. Z.-B. Wang, A. Aldalbahi, T. Ahamad, S.M. Alshehri, P.X. Feng, *Preparation of BiFeO3 and its photoelectric performance as photoanode of DSSC* (Ceramics International, 2021)
41. G. Wei, Z. Xu, X. Zhao, S. Wang, F. Kong, C. An, 2022. N-doped CoSe2 nanomeshes as highly-efficient bifunctional electrocatalysts for water splitting. Journal of Alloys and Compounds 893
42. J. Yang, Y. Niu, J. Huang, L. Liu, X. Qian, 2020. N-doped C/CoSe2@Co–FeSe2 yolk-shell nano polyhedron as superior counter electrode catalyst for high-efficiency Pt-free dye-sensitized solar cell. Electrochimica Acta 330
43. L. Yu, J.F. Yang, X.W.D. Lou, Formation of CoS2Nanobubble Hollow Prisms for Highly Reversible Lithium Storage. Angewandte Chemie - International Edition **55**(43), 13422–13426 (2016)
44. G. Yue, W. Wu, X. Liu, H. Zheng, Enhanced photovoltaic performance of dye-sensitized solar cells based on a promising hybrid counter electrode of CoSe2/MWCNTs. Sol. Energy **167**, 137–146 (2018)

45. K. Zhao, Y. Zhao, M. Hao, X. Li, S. Liu, L. Li, W. Zhang, 2021. Cost effective synthesis Co9S8/Ni9S8 loaded on nitrogen doped porous carbons high efficiency counter electrode materials for liquid thin film solar cells. Electrochimica Acta 399

# Figures

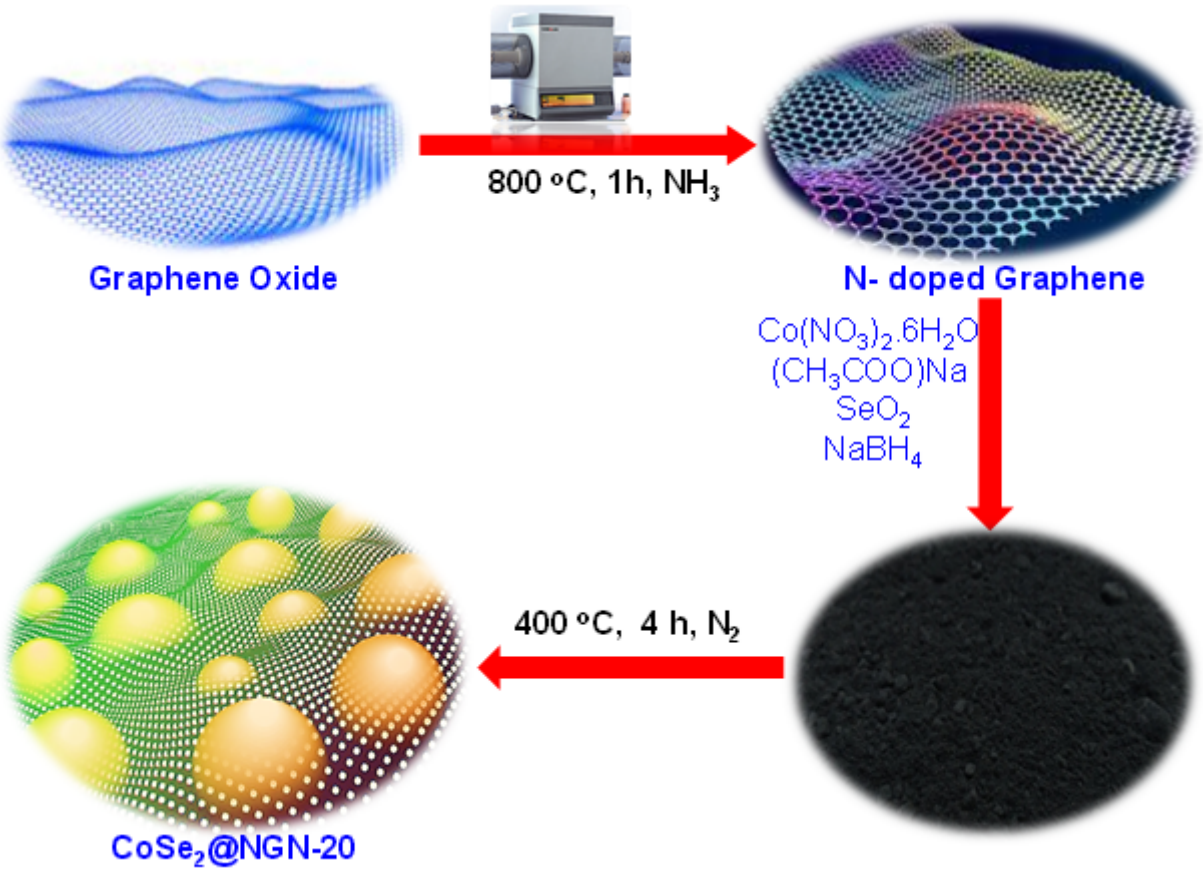


**Figure 1**

The synthesis routes for N-doped graphene and $CoSe_2$@NGN nanocomposite

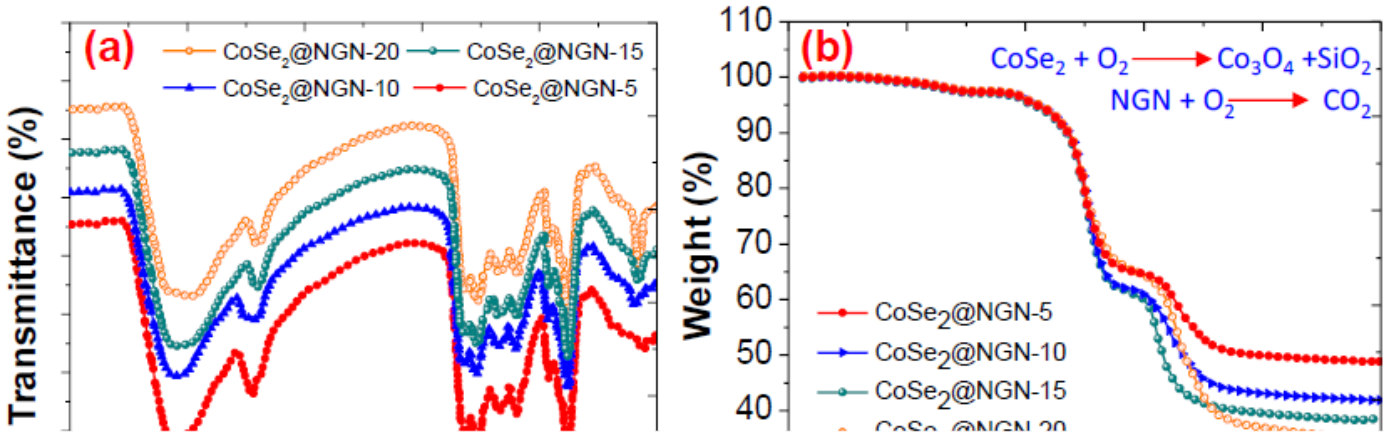


## Figure 2

(a) FTIR spectra and (b) TGA curves (c) XRD spectra of $CoSe_2$@NGNs and (d) Raman spectra of $CoSe_2$@NGNs-15

## Figure 3

(a) SEM image of $CoSe_2$@NGNs-15 (b) TEM image of $CoSe_2$@NGNs-15 (c) HRTEM image of $CoSe_2$@NGNs-15; and (d) HRTEM image and SAED of $CoSe_2$@NGNs-15

## Figure 4

(a): $N_2$ adsorption and desorption isotherm (b) Pore size distribution of the nanocomposites

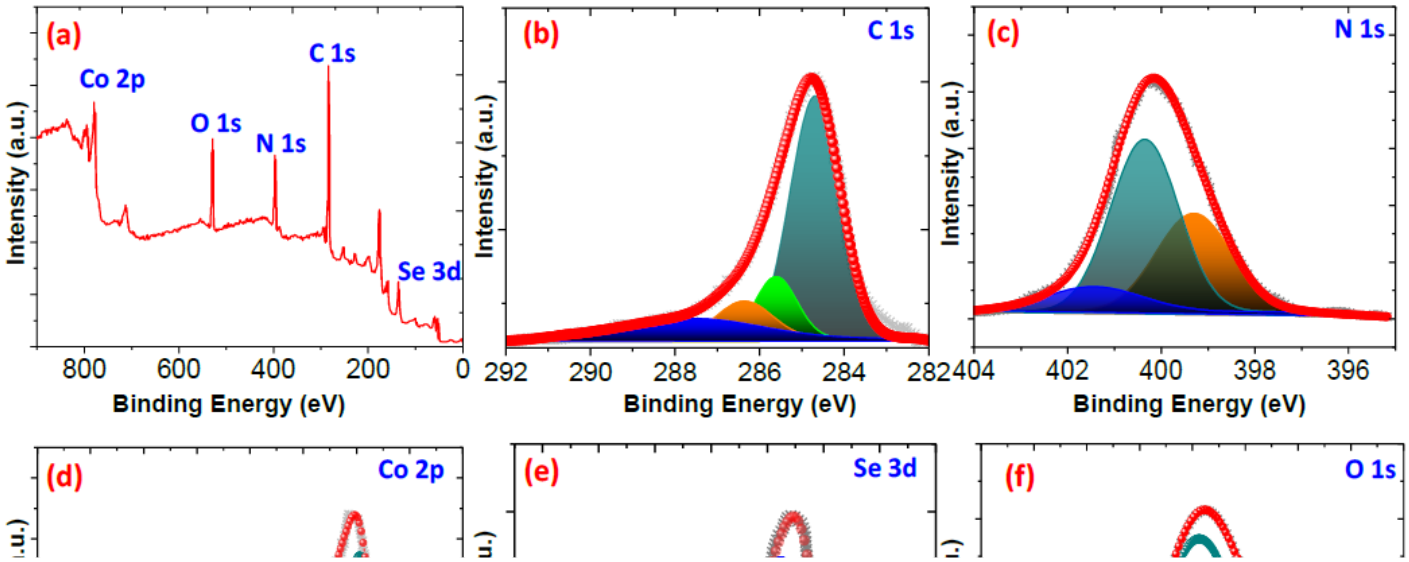


## Figure 5

(a) A wide XPS spectra for the $CoSe_2$@NGNs-15 nanocomposites (b) C1s, (c) N1s (d) Co2p (e) Se3d and (f) O1s

## Figure 6

(a) *J-V* curve and (b) IPCE curve of DSSC with $CoSe_2$@NGN and Pt as the counter electrode

## Figure 7

(a) Schematic diagram of dye-sensitized solar cell (DSSC) assembly

**Figure 8**

(a) Cyclic voltammetry (CV) curves (b) Stability test at scan rate of 50 mv/sec (c) Tafel polarization curves (d) Nyquist EIS plots of DSSC cells with different CEs.

## Supplementary Files

This is a list of supplementary files associated with this preprint. Click to download.

- SupportingInformation.docx